

Controlling the Structure of MoS₂ Membranes via Covalent Functionalization with Molecular Spacers

Eli Hoenig, Steven E. Strong, Mingzhan Wang, Julia M. Radhakrishnan, Nestor J. Zaluzec, J. L. Skinner, and Chong Liu*



Cite This: *Nano Lett.* 2020, 20, 7844–7851



Read Online

ACCESS |

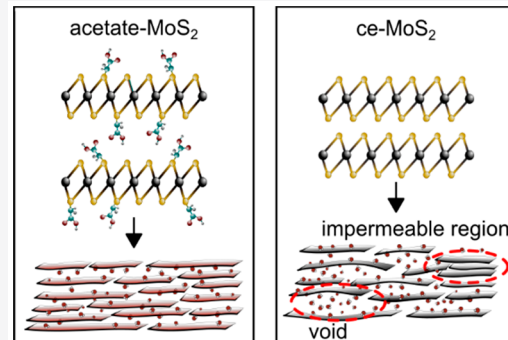
Metrics & More

Article Recommendations

Supporting Information

ABSTRACT: Restacked two-dimensional (2D) materials represent a new class of membranes for water–ion separations. Understanding the interplay between the 2D membrane’s structure and the constituent material’s surface chemistry to its ion sieving properties is crucial for further membrane development. Here, we reveal, and tune via covalent functionalization, the structure of MoS₂-based membranes. We find features on both the ~1 nm (interlayer spacing) and ~100 nm (mesoporous voids between layers) length scales that evolve with the hydration level. The functional groups act as permanent molecular spacers, preventing local impermeability caused by irreversible restacking and promoting the uniform rehydration of the membrane. Molecular dynamics simulations show that the choice of functional group tunes the structure of water within the MoS₂ channel and consequently determines the hydrated interlayer spacing. We demonstrate that MoS₂ membranes functionalized with acetic acid have consistently ~92% rejection of Na₂SO₄ with a flux of ~1.5 lm^{−2} hr^{−1} bar^{−1}.

KEYWORDS: MoS₂, membrane, 2D channel, molecular spacer, interlayer spacing, separation



Restacked two-dimensional (2D) materials, which are assemblies of individual atomically thin sheets with their basal planes lying parallel to each other, comprise a new class of nanofiltration membranes that show great promise as efficient separators of ions and small molecules from water. In a filtration device, water flows through the channels between layers of material with little obstruction, while ions and other small molecules are excluded. Graphene and graphene oxide form the basis for the first molecular sieves^{1–9} but the breadth of constituent materials has grown in recent years to include, among others, boron nitride,¹⁰ MXenes,^{11,12} and transition metal dichalcogenides (TMDs) such as WS₂¹³ and MoS₂.^{14,15} Chemically exfoliated MoS₂ (ce-MoS₂) is a particularly viable candidate for reverse osmosis (RO) desalination, as exemplified in recent studies.^{16–18} The channel width of restacked ce-MoS₂ is on the appropriate length scale for size-based exclusion of ions while facilitating high water flux; furthermore, recent studies have demonstrated that ce-MoS₂ is more structurally stable than its graphene oxide counterpart.^{17,19,20}

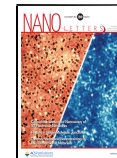
Recent efforts have demonstrated the viability of horizontally aligned ce-MoS₂ as an RO membrane.^{15–18,20} Ries et al. and Hirunpinyopas et al. show that the surface hydrophilicity of MoS₂ membranes has a profound effect on its ion sieving properties.^{16,18} Wang et al. detail the stability of MoS₂ membranes and the relationship between the normalized water flux and applied pressure in a dead-end filtration setup.¹⁷

The interplay of interlayer spacing and surface chemistry and their effects on water and ion transport remain unclear, however. To understand these effects, both single channels and the mesoporous structure of the channel assemblies need to be controlled precisely. Here, we functionalize MoS₂ with molecular spacers and, coupled with a drying and rehydration method, control the structure of MoS₂-based membranes on both the micro- and mesoporous scales. We find features on both length scales that vary with the hydration extent of the membrane and must be considered when rationalizing its filtration properties (Figure 1). With the acetic-acid functionalized MoS₂ (acetate-MoS₂) membranes, we demonstrate consistently high filtration performance: 92(2)% rejection of Na₂SO₄ and 1.5(6) LMH bar flux, higher than acetamide functionalized MoS₂ (amide-MoS₂) and equivalent to carefully tuned ce-MoS₂. Interestingly, acetate-MoS₂ membranes also demonstrate 6.6 fold selectivity of Cu²⁺ over the monovalent cation Na⁺, suggesting the membrane’s possible use for selective ion removal and recovery.

Received: May 21, 2020

Revised: October 1, 2020

Published: October 6, 2020



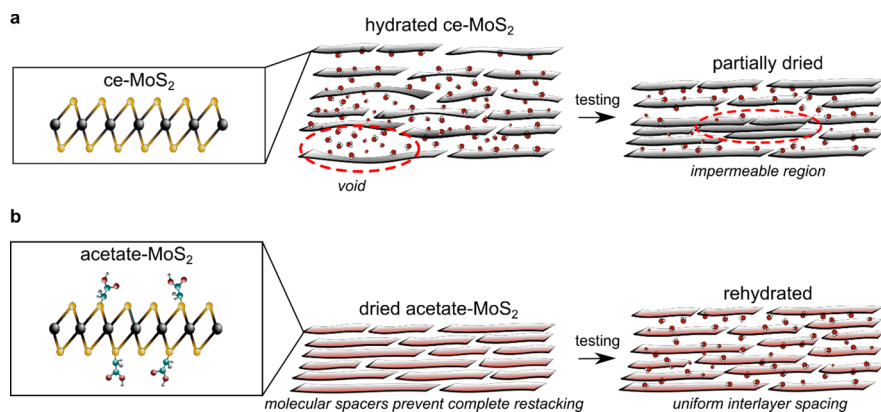


Figure 1. Schematic of the hydration-dependent structure of MoS₂ membranes. (a) Initially, the hydrated ce-MoS₂ membrane is disordered with mesoporous scale voids between layers. When partially dried, the large voids close but parts of the membrane restack to the bulk, decreasing the overall porosity of the membrane (and when completely dried, the membrane is impermeable). (b) Acetate-MoS₂ membranes dry without restacking to the impermeable bulklike structure. This allows the membrane to rehydrate during testing, leading to consistent interlayer spacing with fewer voids or impermeable regions.

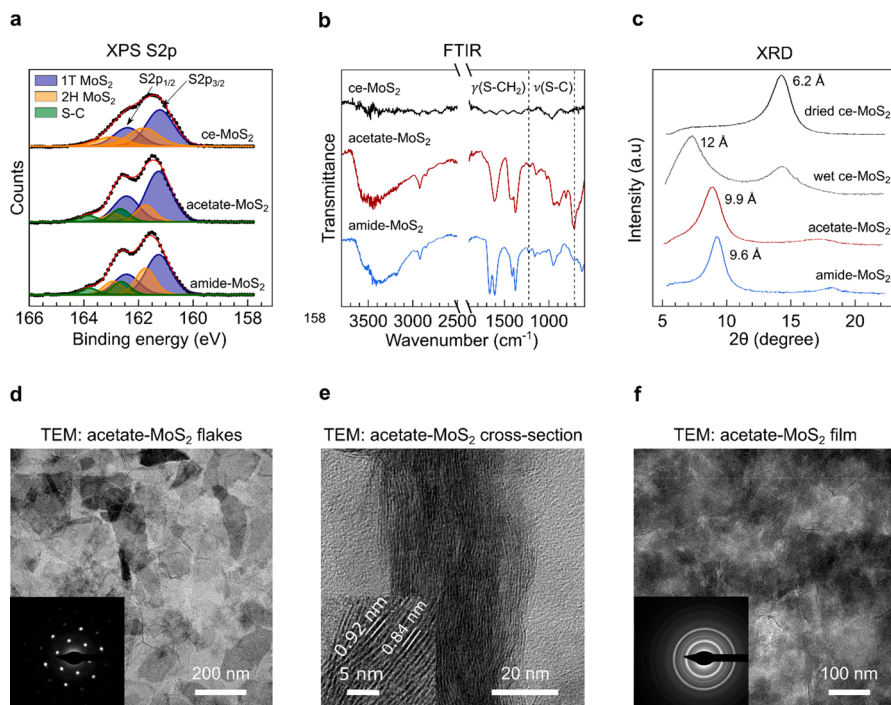


Figure 2. Characterization of functionalized MoS₂. (a) XPS spectra of the S 2p region for ce-, acetate- and amide-MoS₂. The fraction of functional groups is computed by fitting the spectra with peaks from 1T and 2H MoS₂ phases as well as an S-C contribution. (b) FTIR of MoS₂ samples showing the intramolecular acetate and acetamide stretches near 1500 cm⁻¹, and S-CH₂ wagging peaks for acetate- and amide-MoS₂ at 1217 and 1225 cm⁻¹, respectively. Also evident are the S-C stretching peaks at ~715 cm⁻¹.^{25,27} (c) XRD displaying the shift in interlayer spacing for dried functionalized MoS₂ and hydrated ce-MoS₂ relative to dried ce-MoS₂. (d) Top-down TEM of acetate-MoS₂ flakes; the diffraction pattern for a single flake is inset, showing evidence of in-plane hexagonal symmetry. (e) Cross-section TEM image of a 40 nm acetate-MoS₂ membrane. (f) Top-down TEM image of a 50 nm acetate-MoS₂ membrane with the diffraction pattern inset, illustrating the random orientations of a thick composite flake stack.

Further, we explain the effect of molecular functionalization on the interlayer spacing of MoS₂ films using molecular dynamics (MD) simulations. The connection between surface chemistry and membrane structure has previously been attempted using mean field theories that do not account for the layered structure of confined water, which we find is a dominant effect.¹⁷ The MD simulations reveal that the choice of functional group controls the number of water layers within the MoS₂ channel and consequently governs the interlayer spacing and affects water flux. We also find that the diffusion

constant of water molecules varies with functionalization but that this has a modest effect relative to the membrane's physical structure.

RESULTS

Synthesis and Characterization of MoS₂ Based Membranes. An aqueous suspension, shown in Supporting Information (SI) Figure 1a, of ce-MoS₂ flakes is synthesized following the standard lithium-intercalation and exfoliation procedure^{21–23} outlined in Methods (SI). The detailed

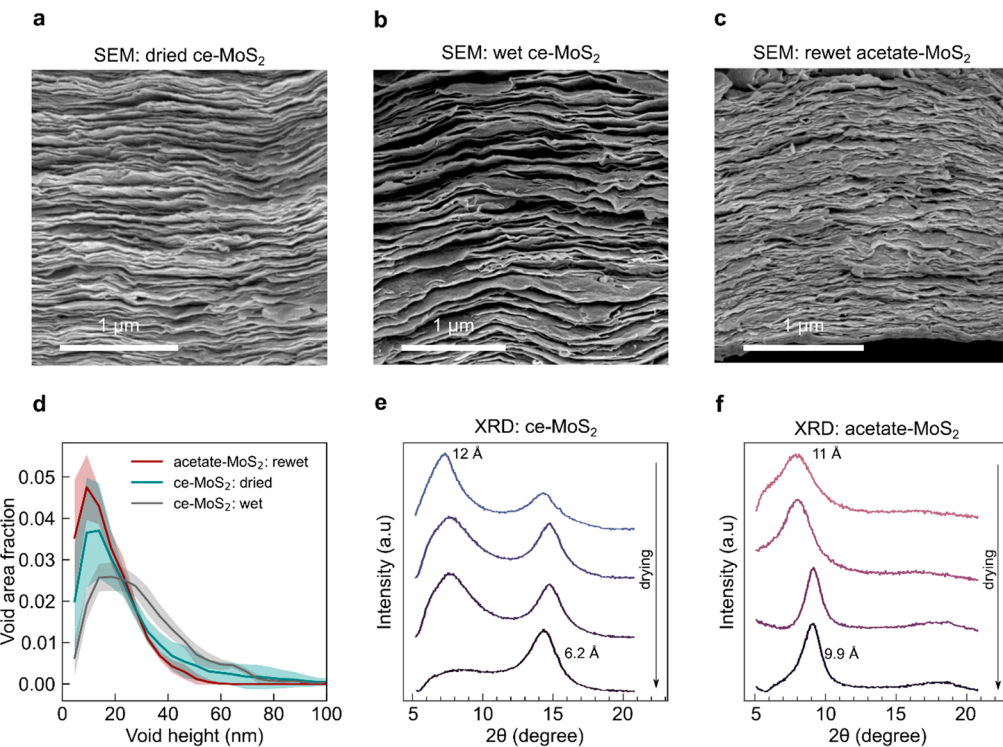


Figure 3. Characterization of membrane structure on the micro- and mesoporous length scales. (a) SEM cross-section of 3 μm thick dried ce-MoS₂ membrane displaying relatively small voids between layers. (b) SEM cross-section of 3 μm freeze-dried ce-MoS₂ membrane; relatively large gaps are visible between layers. (c) SEM cross-section of 2 μm freeze-dried acetate-MoS₂ membrane, dried then rehydrated. (d) Quantification of void height distributions for (a–c). The shaded region depicts the variability between images (shown in SI Figure 6). (e) XRD characterizing the hydration dependent structure of ce-MoS₂ on the microporous scale. As the membrane dries, the bilayer of water peak decreases in intensity, whereas the bulklike peak rises. (f) XRD characterizing the hydration dependent structure of acetate-MoS₂ on the microporous scale, where no bilayer peak is evident.

physical characteristics of individual flakes are provided in Section 1 of Supporting Information. The flakes are generally 100–500 nm in lateral size and only a few nm in total thickness. Membranes are assembled via vacuum filtration on a porous polymer substrate (mixed cellulose ester, 25 nm average pore diameter) and dried for a given period to control the hydration extent.

We covalently functionalize ce-MoS₂ sheets with two small organic molecules: iodoacetic acid and iodoacetamide. We follow the procedure provided in recent studies^{24,25} and outlined in Methods (SI) to graft these organic molecules on MoS₂ flakes. The mechanisms underlying the covalent functionalization are outlined in Section 3 (SI). Importantly, the net negative surface charge of ce-MoS₂ (~0.25 electrons per Mo atom)²⁶ is neutralized during functionalization. Acetic acid, however, deprotonates in neutral pH and induces a net negative charge on the sheet of equal magnitude to that of ce-MoS₂,²⁴ the sheets remain neutral for amide-MoS₂.

The fraction of organic fragments decorating the MoS₂ surface is determined via X-ray photoelectron spectroscopy (XPS) of samples drop cast on Si wafers.^{16,24,25} The degree of functionalization (functional group per Mo atom) is derived from the S 2p region (Figure 2a) as well as the C 1s region, and for amide-MoS₂ the N 1s region.²¹ Using all three methods, the degree of functionalization is calculated to be 20–26% for acetate-MoS₂ and 22–26% for amide-MoS₂ (Section 3 (SI)). These results are well aligned with previous studies.²⁵ More evidence of the covalent nature of the S–C bond on functionalized MoS₂ is provided by attenuated total

reflectance Fourier-transform infrared spectroscopy (FTIR) spectra displayed in Figure 2b.

The structure of MoS₂ membranes on the microporous scale is determined via a combination of XRD and TEM. The interlayer spacing as measured by XRD is 6.2 \AA (bulklike) for dried ce-MoS₂; as shown in Figure 2c, this value grows to 9.9 and 9.6 \AA for dried acetate- and amide-MoS₂, respectively. Flakes of acetate-MoS₂, characterized by TEM in Figure 2d, display similar morphology to and retain the hexagonal in-plane crystal structure of ce-MoS₂ (diffraction pattern shown in inset). A result of this preservation, acetate-MoS₂ membranes have a similar layered structure to that of ce-MoS₂ membranes, only with an expanded interlayer spacing as shown in the TEM cross-section images in Figure 2e and SI Figure 4 (see Methods (SI) for characterization details). When made into membranes, the flakes stack with their basal planes aligned but in random rotational orientations (Figure 2f).

Hydration-Dependent Structure of MoS₂ Based Membranes. Direct visualization of the hydrated MoS₂ membrane structure is accomplished using a standard freeze-drying procedure, outlined in Section 5 (SI). This procedure allows direct morphological comparison between dried ce-MoS₂ (Figure 3a), hydrated ce-MoS₂ (Figure 3b), and rehydrated acetate-MoS₂ (Figure 3c) on the mesoporous scale.

The membrane structure evident in SEM images is similar for rehydrated acetate-MoS₂ and dried ce-MoS₂ but differs for hydrated ce-MoS₂. In rehydrated acetate-MoS₂ and dried ce-MoS₂, the layers are regularly distributed whereas in hydrated ce-MoS₂, the layers are separated by mesoporous scale voids.

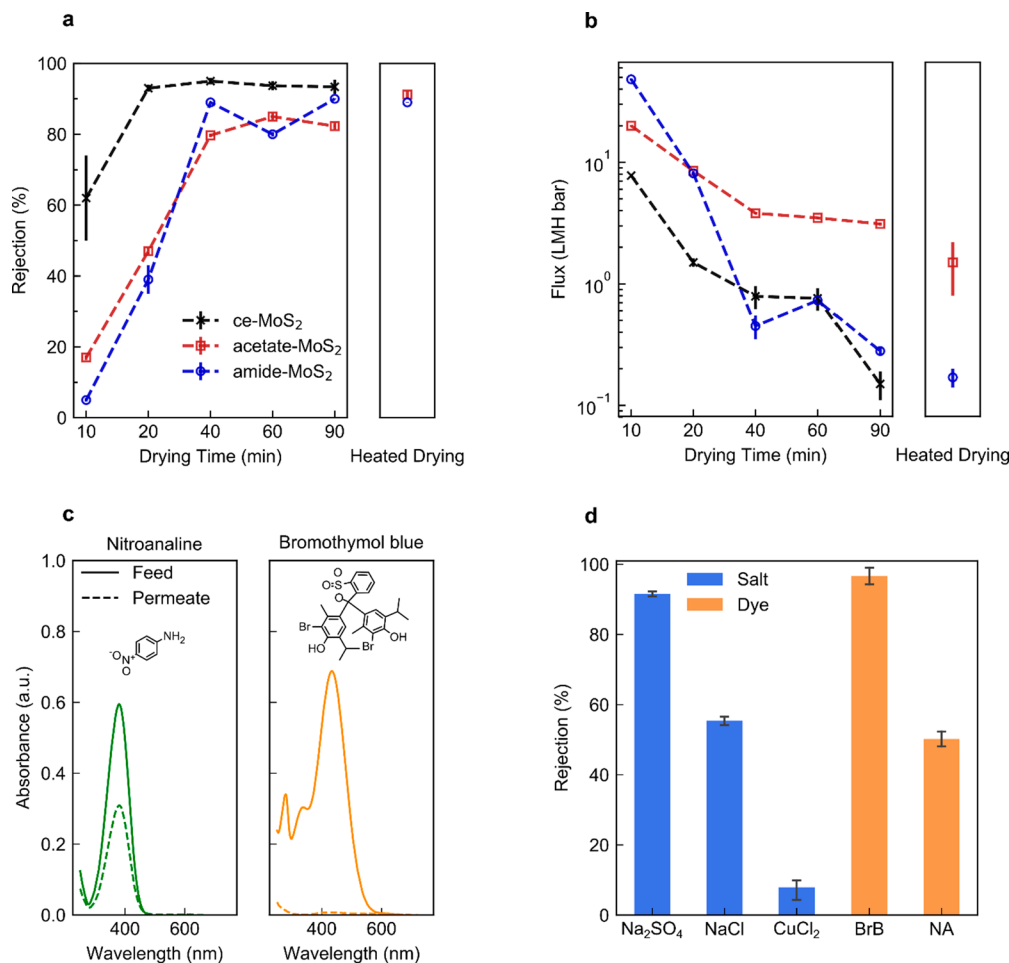


Figure 4. Membrane separation performance: hydration dependent ion rejection (a) and water flux (b) for ce-, acetate-, and amide-MoS₂ in 17 mM Na₂SO₄; water flux and ion rejection for acetate-and amide-MoS₂ prepared by heated drying and rehydrating are also shown. (c) UV-vis spectra of two neutral dyes, NA (molecular size $\sim 4.32 \text{ \AA} \times 6.89 \text{ \AA}$ ²⁸), and BrB at pH = 5.6 ($\sim 10.8 \text{ \AA} \times 13.5 \text{ \AA}$ ²⁹), filtered through acetate-MoS₂ membranes. The spectra for feed and permeate solutions are shown, along with a drawing of the dye molecules to emphasize the size discrepancy. (d) Solute rejection of A₂B (Na₂SO₄), AB (NaCl), and AB₂ (CuCl₂) salts as well as the two neutral dyes, NA and BrB, using acetate-MoS₂ membranes. The rejection between NaCl and CuCl₂ indicates a 6.6-fold selectivity of Cu²⁺ to Na⁺.

The qualitative structure of these membranes is consistent throughout a given membrane and between membranes (SI Figure 6). A quantitative depiction of the void height distribution (see Section 6 (SI) for procedural details) is shown in Figure 3d; as expected, hydrated ce-MoS₂ displays a broader peak at larger values ($\sim 20 \text{ nm}$) compared to dried ce-MoS₂ and acetate-MoS₂ ($\sim 10 \text{ nm}$). From this result, we conclude that with partial drying or surface functionalization and rehydration, the size of mesoporous scale voids is reduced.

The evolving mesoporous scale morphology is accompanied by evolving structure on the microporous scale. As shown in the XRD spectra in Figure 3e, in wet ce-MoS₂, two peaks are apparent corresponding to the bulk (6.2 \AA) and hydrated (12 \AA) interlayer spacings. As the membrane dries, the XRD peak corresponding to 12 \AA interlayer spacing decreases in intensity while the peak at 6.2 \AA increases. This evolution indicates irreversible stacking to bulk MoS₂. In contrast, no bulk peak (6.2 \AA) is ever present in acetate-MoS₂ (Figure 3f) or amide-MoS₂ (SI Figure 7); the singular channel width for acetate-MoS₂ simply shifts to smaller values as water leaves the membrane (from 11 to 9.9 \AA).

Separation Performance of MoS₂ Based Membranes.

The evolving structure of ce-MoS₂ membranes dramatically

affects separation performance, as indicated by the dependence of water flux and ion rejection on membrane drying time. To detail this association, membranes are dried for a defined period in room-temperature conditions (humidity 20–30%) after fabrication, then loaded in a stirred, pressure-assisted dead-end filtration cell for tests. All samples are tested in brackish water conditions with 17 mM (~2500 ppm) Na₂SO₄ under pressures of 150 psi (10.3 bar). The performance metrics are measured until the ion rejection stabilizes. Acetate-MoS₂ membranes are also tested against 34 mM (2000 ppm) NaCl and 17 mM (~2300) ppm CuCl₂, the neutral dyes 4-nitroaniline (NA) and bromothymol blue (BrB).

The ion rejection of ce-MoS₂ membranes increases within the initial drying period but subsequently remains constant (Figure 4a); the flux, on the other hand, decreases by 2 orders of magnitude as a function of drying time (Figure 4b). We associate the initial increase in rejection with the closure of percolating voids. Once these voids are closed, no further increase in ion rejection is expected despite lower water flux values; restacking to bulk entirely seals off portions of the membrane instead of forming smaller water channels. By tuning the drying time (to the minute) ce-MoS₂ membranes can display performance as high as 95(1)% rejection of

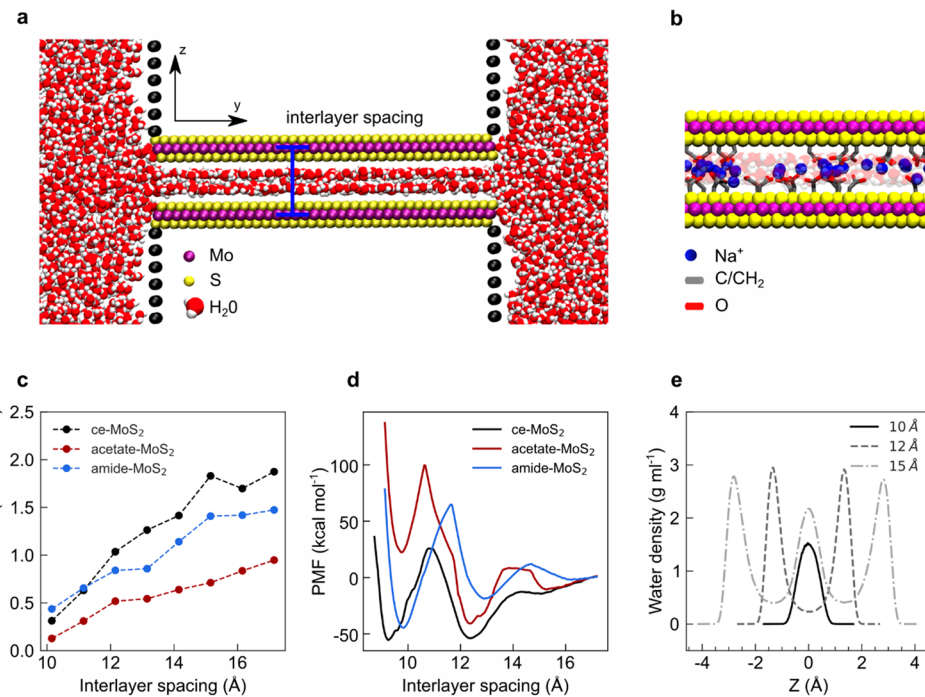


Figure 5. MD simulations describing the dynamics and structure of water in membranes. (a) MD simulation snapshot showing water confined in a MoS₂ channel with 12 Å interlayer spacing (center-to-center Mo–Mo distance). (b) Cross section of acetate-MoS₂ with functional groups placed randomly at 0.2 per Mo atom, (c) The diffusion constant of water in ce-, acetate-, and amide-MoS₂ channels as a function of interlayer spacing. (d) PMF as a function of interlayer spacing for ce-, acetate-, and amide-MoS₂. (e) The density of water as a function of the z-coordinate in an acetate-MoS₂ channel. Here, we show profiles for interlayer spacings that exhibit clearly resolved water layering.

Na₂SO₄ with 0.8(2) LMH bar water flux. Even though ce-MoS₂ shows great potential for ion separations, the transient membrane structure makes the membrane hard to preserve for practical applications.

The drying-dependent performance of acetate-MoS₂ differs qualitatively from that of ce-MoS₂. The ion rejection plateaus more slowly for acetate-MoS₂ membranes (Figure 4a). Furthermore, when the membrane is dried completely by heating at 60 °C for 4 h, after rehydration during testing, water flows at 1.5(6) LMH bar while the ion rejection reaches 92(2)% (ce-MoS₂ membranes dried under the same conditions are impermeable). Furthermore, the flux of acetate-MoS₂ decays at a much slower rate (and eventually appears to plateau) relative to that of ce-MoS₂, which nearly halves in 15 h (SI Figure 9). This result suggests that functionalizing MoS₂ with acetate ions is a reliable method to achieve high rejection of divalent anions, only transiently attainable via partial drying of ce-MoS₂. The amide-MoS₂ membranes exhibit smaller flux at long drying times relative to acetate-MoS₂. They do remain permeable after complete drying, however, unlike the ce-MoS₂ membranes; dried amide-MoS₂ membranes exhibit 89.0(1)% rejection with a flux of 0.7(2) LMH bar.

We test acetate-MoS₂ membranes against two different neutral dyes in order to isolate the size sieving from the electrostatic repulsion effects on solute rejection (Figure 4c). Acetate-MoS₂ rejects the large neutral dye molecule BrB (molecular size ~10.8 Å × 13.5 Å²⁹) with an efficacy of 98%, but only partially impedes the permeation of the smaller neutral molecule NA (~4.32 Å × 6.89 Å²⁸), corroborating the import of the size sieving effect (Figure 4d). We also measure the rejection of NaCl and CuCl₂ (Figure 4d). Interestingly, CuCl₂ is barely impeded by acetate-MoS₂ membranes, likely a

result of both the slightly smaller hydrated radius of Cu²⁺ compared to Na⁺ and SO₄²⁻ and its overall charge.³⁰ We note the selectivity toward divalent cations over monovalent cations measured here (calculated as the reciprocal of the ratio of CuCl₂ and NaCl rejection) is ~6.6, higher than that of recent studies of 2D materials, which report divalent over monovalent cation selectivity of ~1–1.9.^{31–33} In commercial Nafion ion exchange membranes, the selectivity is typically reversed, with monovalent cations preferentially transported over divalent cations.³⁴ We compare the separation performance of acetate-MoS₂ membranes to existing literature in SI Figure 13 for NaCl and Na₂SO₄.

The dependence of water flux on MoS₂ surface treatment is a result of differing water diffusion constants within membrane channels and varying membrane porosities. Diffusion constants are calculated via MD simulations discussed in the subsequent section; porosity is determined by structure of MoS₂ membranes on the microporous and mesoporous scales. As depicted in SI Figure 10, ce-MoS₂ partially restacks to bulk, decreasing the effective porosity of the membrane, whereas the acetate- and amide-MoS₂ channels remain uniformly open. The different behaviors demonstrated by amide-MoS₂ and acetate-MoS₂ are likely a result of their differing hydrophilicities (SI Figure 11); functionalization with acetic acid (acetamide) increases (decreases) the hydrophilicity relative to that of ce-MoS₂. Consequently, the interlayer spacing of acetate-MoS₂ increases to a greater extent relative to that of amide-MoS₂ when rehydrated, as shown in SI Figure 10. In the following sections, we employ MD simulations to provide a quantitative description of the microporous structure of ce- and functionalized MoS₂ that rationalizes with greater detail each sample's equilibrium hydrated interlayer spacing.

MD Simulations: Water Dynamics in MoS₂ Channels. To elucidate the factors contributing to water diffusion in ce- and functionalized MoS₂, we conduct MD simulations on single channels formed by parallel MoS₂ sheets (the setup is shown in Figure 5a). By characterizing the water structure and dynamics at a sequence of interlayer spacings for ce-, acetate- and amide-MoS₂, we cover the entire parameter space attainable in our experiments. To probe the effects of surface modification, we decorate the MoS₂ sheets with functional groups at a similar density to that measured experimentally (Figure 5b).

To compare water flux between samples, we compute the diffusion constant (derived from the mean squared displacement of water molecules in the MoS₂ channel) for interlayer spacings from 10 to 17 Å. We find that for a 12 Å interlayer spacing, the diffusion constant varies with surface chemistry as ce-MoS₂ > amide-MoS₂ > acetate-MoS₂ (Figure 5c). We attribute the lower diffusion constants for acetate-MoS₂ and amide-MoS₂ partially to steric obstruction arising from the functional groups extruding from the MoS₂ surface. Given consistent interlayer spacing and mesoscale morphology for all membrane surface chemistries tested here, our MD simulations indicate that ce-MoS₂ should exhibit the fastest water flux. Experimentally, however, ce- and acetate-MoS₂ have equivalent hydrated interlayer spacings (12 Å) but acetate-MoS₂ demonstrates the highest water flux. This result suggests that the restacking to bulk behavior effectively reduces the porosity of the membrane (or increases the tortuosity), leading to reductions in flux that overcome the marginally larger diffusion constant for ce-MoS₂ relative to functionalized MoS₂. The reduced flux of amide-MoS₂ relative to acetate-MoS₂ likely derives from its smaller interlayer spacing in the hydrated state. An analytical relationship between these morphological factors and the total water flux through the MoS₂ membranes tested here is provided in Section 15 of Supporting Information.

MD Simulations: Water Structure and Interlayer Spacing. The equilibrium spacing between MoS₂ sheets in an aqueous medium governs the ion rejection and water flux through the membranes assembled from those sheets. The equilibrium spacing is determined by the complex interplay of electrostatic and van der Waals interactions in addition to hydration forces arising from the confinement of water in the MoS₂ channel.³⁵ To quantify the sum of these interactions, we use umbrella sampling to calculate the potential of mean force (PMF) as a function of interlayer spacing (Figure 5d). This approach captures the effects of water structure on the interlayer spacing at the subnanometer scale, the details of which are not included in models such as extended DLVO theory.^{17,35} While our model, which is parametrized to capture water–water and water–MoS₂ interactions, may break down at small interlayer spacings where MoS₂–MoS₂ interactions dominate, at the spacings of interest here the MoS₂ interactions are largely mediated by water molecules and hydration forces dominate³⁵ (see SI Figure 15).

The PMF profiles depicted in Figure 5d display clear minima at around 9–10 and 12–13 Å, but the relative depths of these two minima vary dramatically with surface functionalization. As detailed in Section 17 (SI), these minima and their relative depths explain the stability and value of the interlayer spacing of ce- and functionalized MoS₂ membranes in aqueous media. The structure of the PMFs in Figure 5d can be interpreted in terms of interactions in the system at the molecular level. The overall oscillatory structure is well understood and is a result of

the discrete nature of the water layers confined within the channel.^{35–37} To illustrate this, we compute the water density profile along the membrane normal at fixed interlayer spacings between 10 and 17 Å (SI Figure 16). The minima in the PMF profiles at around 10, 12.5, and 15 Å correspond to one, two, and three layers of water inside the channel, respectively; this is shown for acetate-MoS₂ in Figure 5e.

Given that hydrated ce- and acetate-MoS₂ membranes have experimental interlayer spacings of 12 Å, the density profiles in Figure 5e and SI Figure 16 indicate that each MoS₂ sheet adsorbs a single layer of water approximately 2 Å thick. We conclude that a bilayer of water occupies each channel, as hypothesized in prior studies.^{16,17,19,38,39} These results also indicate that the steric effects of functional groups decorating the MoS₂ surface are secondary to that of the structure of water within the MoS₂ channel; within our current experimental setup, the interlayer spacing can only take on discrete values corresponding to an integer number of water layers. It remains an open question whether a greater degree of functionalization ($\gg 20\%$) might destroy the ordering of the water, thereby reducing the hydration forces and permitting finer control over the interlayer spacing. However, this will likely also reduce the flux due to the density of functional groups in the channel.

■ DISCUSSION

We have shown that the ion sieving properties of MoS₂ membranes can be tuned by varying the degree of hydration. We have also demonstrated that membrane functionalization with acetic acid groups is a promising route toward consistently achieving high salt rejection and water flux. Direct evidence of the effect of surface charge would be useful to evaluate the efficacy of alternative functional groups but would require complete decoupling of surface charge from membrane morphology. Increasing the water flux of acetate-MoS₂ membranes could be realized by employing thinner films with less surface topography; this may be accomplished through synthesis of larger and more uniform flakes, employing a smoother substrate, or through alternative fabrication techniques.⁴⁰

MD simulations have revealed the structure of water within the membrane that forms the basis for its hydration-dependent structure. In addition, the trends derived from these MD simulations corroborate the dominance of the rehydration behavior of MoS₂ membranes in separation tests and emphasize the importance of water structure on both the microporous and mesoporous scales. Our work provides structural and chemical information on MoS₂ membranes, providing insight into their behavior as separation membranes or when employed in nanofluidic platforms or even as electrode materials.

■ ASSOCIATED CONTENT

SI Supporting Information

The Supporting Information is available free of charge at <https://pubs.acs.org/doi/10.1021/acs.nanolett.0c02114>.

Additional membrane synthesis and characterization details as well as dead-end filtration test results, such as long-term flux stability and thickness-dependent performance; supporting and methodological details for MD simulations, and the derivation of the analytical relationship connecting these simulations to observed data (PDF)

AUTHOR INFORMATION

Corresponding Author

Chong Liu — Pritzker School of Molecular Engineering,
University of Chicago, Chicago, Illinois 60637, United States;
orcid.org/0000-0003-4851-7888; Email: chongliu@uchicago.edu

Authors

Eli Hoenig — Pritzker School of Molecular Engineering,
University of Chicago, Chicago, Illinois 60637, United States
Steven E. Strong — Pritzker School of Molecular Engineering,
University of Chicago, Chicago, Illinois 60637, United States
Mingzhan Wang — Pritzker School of Molecular Engineering,
University of Chicago, Chicago, Illinois 60637, United States;
orcid.org/0000-0003-1956-9769
Julia M. Radhakrishnan — Pritzker School of Molecular
Engineering, University of Chicago, Chicago, Illinois 60637,
United States
Nestor J. Zaluzec — Photon Science Division, Argonne National
Laboratory, Lemont, Illinois 60439, United States
J. L. Skinner — Pritzker School of Molecular Engineering,
University of Chicago, Chicago, Illinois 60637, United States

Complete contact information is available at:

<https://pubs.acs.org/10.1021/acs.nanolett.0c02114>

Author Contributions

C.L. and E.H. conceived the idea. J.S. and S.S. carried out and interpreted the molecular dynamics simulations. E.H. contributed to all of the experimental work. M.W. contributed to the experimental work related to membrane testing and material characterization. J.R. contributed to experimental work related to material synthesis. N.J.Z. assisted with TEM characterization. E.H., S.S., J.S., and C.L. analyzed the data and cowrote the paper. All authors discussed the whole paper.

Notes

The authors declare no competing financial interest.

ACKNOWLEDGMENTS

This work is supported by the Pritzker School of Molecular Engineering and the Research Computing Center at the University of Chicago and the Advanced Materials for Energy-Water-Systems (AMEWS) Center, an Energy Frontier Research Center funded by the U.S. Department of Energy, Office of Science, Basic Energy Sciences. It also employed resources in the Center for Nanoscale Materials, an Office of Science user facility at Argonne National Laboratory under Contract No. DE-AC02-06CH11357. We acknowledge Grant Hill, Adarsh Suresh, and Guiming Peng for their insightful comments.

REFERENCES

- (1) Chen, L.; et al. Ion sieving in graphene oxide membranes via cationic control of interlayer spacing. *Nature* **2017**, *550*, 380–383.
- (2) Hu, M.; Mi, B. Enabling graphene oxide nanosheets as water separation membranes. *Environ. Sci. Technol.* **2013**, *47*, 3715–3723.
- (3) Joshi, R. K.; et al. Precise and ultrafast molecular sieving through graphene oxide membranes. *Science* **2014**, *343*, 752–754.
- (4) Liu, T.; et al. Regulating the interlayer spacing of graphene oxide membranes and enhancing their stability by use of PACl. *Environ. Sci. Technol.* **2019**, *53*, 11949–11959.
- (5) Morelos-Gomez, A.; et al. Effective NaCl and dye rejection of hybrid graphene oxide/graphene layered membranes. *Nat. Nanotechnol.* **2017**, *12*, 1083–1088.

(6) Nair, R. R.; Wu, H. A.; Jayaram, P. N.; Grigorieva, I. V.; Geim, A. K. Unimpeded permeation of water through helium-leak-tight graphene-based membranes. *Science* **2012**, *335*, 442–444.

(7) Sahu, S.; Zwolak, M. Ionic selectivity and filtration from fragmented dehydration in multilayer graphene nanopores. *Nanoscale* **2017**, *9*, 11424–11428.

(8) Surwade, S. P.; et al. Water desalination using nanoporous single-layer graphene. *Nat. Nanotechnol.* **2015**, *10*, 459–464.

(9) Raidongia, K.; Huang, J. Nanofluidic ion transport through reconstructed layered materials. *J. Am. Chem. Soc.* **2012**, *134*, 16528–16531.

(10) Chen, C.; et al. Functionalized boron nitride membranes with ultrafast solvent transport performance for molecular separation. *Nat. Commun.* **2018**, *9*, 1–8.

(11) Ren, C. E.; et al. Charge- and size-selective ion sieving through $Ti_3C_2T_x$ MXene membranes. *J. Phys. Chem. Lett.* **2015**, *6*, 4026–4031.

(12) Ding, L.; Wei, Y.; Li, L.; Zhang, T.; Wang, H.; Xue, J.; Ding, L.-X.; Wang, S.; Caro, J.; Gogotsi, Y. MXene molecular sieving membranes for highly efficient gas separation. *Nat. Commun.* **2018**, *9*, 1–7.

(13) Sun, L.; et al. Ultrafast molecule separation through layered WS_2 nanosheet membranes. *ACS Nano* **2014**, *8*, 6304–6311.

(14) Liu, G.; Jin, W.; Xu, N. Two-dimensional-material membranes: a new family of high-performance separation membranes. *Angew. Chem., Int. Ed.* **2016**, *55*, 13384–13397.

(15) Sun, L.; Huang, H.; Peng, X. Laminar MoS_2 membranes for molecule separation. *Chem. Commun.* **2013**, *49*, 10718–10720.

(16) Ries, L.; et al. Enhanced sieving from exfoliated MoS_2 membranes via covalent functionalization. *Nat. Mater.* **2019**, *18*, 1112–1117.

(17) Wang, Z.; et al. Understanding the aqueous stability and filtration capability of MoS_2 membranes. *Nano Lett.* **2017**, *17*, 7289–7298.

(18) Hirunpinyopas, W.; et al. Desalination and nanofiltration through functionalized laminar MoS_2 membranes. *ACS Nano* **2017**, *11*, 11082–11090.

(19) Zheng, S.; Tu, Q.; Urban, J. J.; Li, S.; Mi, B. Swelling of graphene oxide membranes in aqueous solution: characterization of interlayer spacing and insight into water transport mechanisms. *ACS Nano* **2017**, *11*, 6440–6450.

(20) Deng, M.; Kwac, K.; Li, M.; Jung, Y.; Park, H. G. Stability, molecular sieving, and ion diffusion selectivity of a lamellar membrane from two-dimensional molybdenum disulfide. *Nano Lett.* **2017**, *17*, 2342–2348.

(21) Eda, G.; et al. Photoluminescence from chemically exfoliated MoS_2 . *Nano Lett.* **2011**, *11*, 5111–5116.

(22) Joensen, P.; Frindt, R. F.; Morrison, S. R. Single-layer MoS_2 . *Mater. Res. Bull.* **1986**, *21*, 457–461.

(23) Zheng, J.; et al. High yield exfoliation of two-dimensional chalcogenides using sodium naphthalenide. *Nat. Commun.* **2014**, *5*, 2995.

(24) Paredes, J. I.; et al. Impact of covalent functionalization on the aqueous processability, catalytic activity, and biocompatibility of chemically exfoliated MoS_2 nanosheets. *ACS Appl. Mater. Interfaces* **2016**, *8*, 27974–27986.

(25) Voiry, D.; et al. Covalent functionalization of monolayered transition metal dichalcogenides by phase engineering. *Nat. Chem.* **2015**, *7*, 45–49.

(26) Heising, J.; Kanatzidis, M. G. Exfoliated and restacked MoS_2 and WS_2 : ionic or neutral species? encapsulation and ordering of hard electropositive cations. *J. Am. Chem. Soc.* **1999**, *121*, 11720–11732.

(27) Socrates, G. *Infrared and Raman characteristic group frequencies: tables and charts*; 3rd ed.; John Wiley & Sons: Chichester, U.K., 2001.

(28) Zhang, W.; Zhang, L.; Zhao, H.; Li, B.; Ma, H. A two-dimensional cationic covalent organic framework membrane for selective molecular sieving. *J. Mater. Chem. A* **2018**, *6*, 13331–13339.

(29) Gadwal, I.; et al. Synthesis of Sub-10 nm Two-Dimensional Covalent Organic Thin Film with Sharp Molecular Sieving Nanofiltration. *ACS Appl. Mater. Interfaces* **2018**, *10*, 12295–12299.

- (30) Marcus, Y. Ionic radii in aqueous solutions. *Chem. Rev.* **1988**, *88*, 1475–1498.
- (31) Akbari, A.; Sheath, P.; Martin, S. T.; Shinde, D. B.; Shaibani, M.; Banerjee, P. C.; Tkacz, R.; Bhattacharyya, D.; Majumder, M. Large-area graphene-based nanofiltration membranes by shear alignment of discotic nematic liquid crystals of graphene oxide. *Nat. Commun.* **2016**, *7*, 10891.
- (32) Han, R.; Wu, P. High-performance graphene oxide nanofiltration membrane with continuous nanochannels prepared by the in situ oxidation of MXene. *J. Mater. Chem. A* **2019**, *7*, 6475–6481.
- (33) Han, Y.; Jiang, Y.; Gao, C. High-flux graphene oxide nanofiltration membrane intercalated by carbon nanotubes. *ACS Appl. Mater. Interfaces* **2015**, *7*, 8147–8155.
- (34) Goswami, A.; Acharya, A.; Pandey, A. K. Study of Self-Diffusion of Monovalent and Divalent Cations in Nafion-117 Ion-Exchange Membrane. *J. Phys. Chem. B* **2001**, *105*, 9196–9201.
- (35) Israelachvili, J. N.; McGuiggan, P. M. Forces Between Surfaces in Liquids. *Science* **1988**, *241*, 795–800.
- (36) Wallqvist, A.; Berne, B. J. Computer simulation of hydrophobic hydration forces on stacked plates at short range. *J. Phys. Chem.* **1995**, *99*, 2893–2899.
- (37) Chávez-Páez, M.; Van Workum, K.; de Pablo, L.; de Pablo, J. J. Monte carlo simulations of Wyoming sodium montmorillonite hydrates. *J. Chem. Phys.* **2001**, *114*, 1405–1413.
- (38) Joensen, P.; Crozier, E. D.; Alberding, N.; Frindt, R. F. A study of single-layer and restacked MoS₂ by X-ray diffraction and X-ray absorption spectroscopy. *J. Phys. C: Solid State Phys.* **1987**, *20*, 4043–4053.
- (39) Kwac, K.; et al. Multilayer two-dimensional water structure confined in MoS₂. *J. Phys. Chem. C* **2017**, *121*, 16021–16028.
- (40) Mahalingam, D. K.; Wang, S.; Nunes, S. P. Graphene oxide liquid crystal membranes in protic ionic liquid for nanofiltration. *ACS Appl. Nano Mater.* **2018**, *1*, 4661–4670.